Hindawi
Mobile Information Systems
Volume 2022, Article ID 9396102, 11 pages
https://doi.org/10.1155/2022/9396102

Research Article

Recognition and Detection of Vehicle Noise and Vibration Signals Relying on Variable Step Size LMS Algorithm

Rujia Wang

School of Automobile and Traffic Engineering, Jiangsu University of Technology, Changzhou, Jiangsu, China 213001

Correspondence should be addressed to Rujia Wang; 2020655177@smail.jsut.edu.cn

Received 16 February 2022; Revised 21 March 2022; Accepted 28 March 2022; Published 23 April 2022

Academic Editor: Hye-jin Kim

Vehicle interior noise is a harmful sound formed in the vehicle interior under the influence of engine noise, transmission system noise, and body radiation noise during vehicle operation. The intensity of noise in the vehicle increases with the increase of vehicle speed and engine speed, which worsens the operating environment of the vehicle and does harm to the mood, spirit, and physiology of drivers and passengers. Because the noise is difficult to identify in the process of vehicle vibration signal recognition, aiming at the problem of vehicle vibration signal detection under the background of strong noise, combined with the characteristics of vehicle vibration signal, the variable step size LMS algorithm is applied to vehicle noise and vibration signal recognition. In this paper, based on the signal eigenvalues obtained from the vibration signal characteristics in the noise and vibration signal, the eigenvalues of the vehicle noise can be extended from the frequency domain to the complex plane through the operation of the variable step size LMS, and the separation law corresponding to the extended vibration intensity can be used at the same time. It is used to obtain data by the signal variable step size LMS algorithm, and the obtained optimal separability feature is used as the characteristic parameter of the vibration signal. Finally, the results of an example analysis show that the algorithm proposed in this paper can be used to identify different types of vehicle noise and vibration signals, has a certain anti-interference performance against noise, and can improve the recognition rate of vehicle noise and vibration signals.

1. Introduction

Vibration signal recognition is one of the key methods in the vehicle noise and vibration signal recognition industry. It has been widely used in various fields. The signal, as a carrier of information and data transmission, contains the characteristics of noise interference, which can realize the accurate identification and detailed analysis of vehicle noise and vibration signals, obtain the characteristics of vehicle noise and vibration signals, and provide a basis for the effective identification of subsequent vehicle noise and vibration signals [1]. Currently, in order to accurately identify the noise and vibration signals of the vehicle, the characteristics of the vibration signal of the vehicle noise and vibration signal are generally selected to comply with the characteristics of no change in time shift, no change in size, and no change in phase. On the basis of meeting the above conditions, signal noise vibration signal analysis also needs to maintain high antinoise performance and has been widely used in different industries. Because the noise and vibration signal analysis process is relatively simple, the amount of computation is less, and the high-order spectrum analysis characteristics are maintained simultaneously, so this signal analysis process is widely used in the field of vehicle noise and vibration signal processing.

As one of the key methods in the current vehicle driving industry, vehicle noise and vibration signal recognition has been widely used in various industries and military fields. As the carrier of information data transmission, the signal contains the characteristics of the radiation source, which can realize the accurate identification and detailed analysis of the vehicle noise and vibration signals and obtain the bispectral characteristics of the vehicle driving radiation source, which provides a basis for the effective identification of the subsequent vehicle noise and vibration signal radiation source [2, 3]. In order to accurately identify the vehicle noise

and vibration signal, the bispectral characteristics of the vehicle noise and vibration signals are generally selected to comply with the characteristics of no change in the time shift, size, and phase. Signal bispectral analysis not only needs to meet the above conditions but also needs to maintain high antinoise performance and has been widely used in different industries. Since the bispectral analysis process is relatively simple, the amount of computation is less, and the high-order spectrum analysis characteristics are maintained simultaneously, so it is widely used in the field of vehicle noise and vibration signal processing. Based on the bispectral quadratic feature of vehicle noise and vibration signals in the root system, the bispectral quadratic feature of the complex diagonal tangent of the signal is obtained. Due to the different recognition accuracy of high-performance computing subpaths, the variable step LMS algorithm can be used to obtain the eigenvectors of vehicle noise and vibration signals from the high-performance computing results [4–6]. Due to the problem of noise and vibration signal recognition during vehicle driving, the variable step LMS algorithm is applied to the vehicle noise and vibration signal recognition algorithm. According to the signal eigenvalues obtained by the diagonal slice bispectrum in the noise vibration signal, the Chiro-Z operation can be used to extend the eigenvalues of the bispectral diagonal slices from the frequency domain to the complex plane, and meanwhile, the separating degree law corresponding to extended Bhattacharyya distance is used, to obtain data with the signal variable step size LMS algorithm, and the optimal separable degree feature obtained is used as the bispectral feature parameter value, and the support vector machine is used for testing simultaneously [7]. The radiation source noise is mainly caused by the transmitter noise during the driving process of the vehicle, which generally refers to the abnormal changes caused by the amplitude, frequency, pulse width, and repetition frequency of the vehicle noise vibration signal; that is, the noise from the radiation source is resulted from the stability of the signal during the vehicle driving process. Signal instability can be roughly divided into two types: regularity and randomness [8, 9]. The instability of regularity is mainly caused by insufficient power supply filtering and mechanical jitter. Random instability is caused by the noise generated by the transmitter tube and the random jitter of the modulated pulse. Nowadays, the standards for vehicle noise and vibration signals are gradually improving, and at the same time, the requirements for the stability of the transmitter are also increased. Therefore, the large-scale use of main vibration amplifying transmitters will generate noise mainly in the following three aspects: (1) frequency domain distortion due to the amplitude-frequency characteristics and phase characteristics of the amplification chain. (2) The top of the modulated pulse vibrates and the top begins to drop, which corresponds to the time-domain distortion phenomenon caused by the parasitic phase or amplitude of the signal caused by the power supply fluctuation of the transmitter. (3) Due to the insufficient frequency stability of the main control oscillator, the phase stability is insufficient. Due to the different circuits or devices used by different vehicle running transmitters, the noise of different vehicles running transmitters is different. Therefore, the incompatible modulation of the vehicle noise vibration signal pulse is due to the transmitter noise, because the noise is caused by different kinds of spurious modulation. Vehicle noise and vibration signals present different signal characteristics [10, 11].

In this paper, based on the vibration intensity of the vehicle noise and vibration signal, the vibration intensity of the signal paired noise signal is obtained. Due to the different recognition accuracy of different high-performance computing subpaths, the variable step LMS algorithm can be used to obtain the eigenvectors of vehicle noise and vibration signals according to the high-performance computing results. The final experimental results show that the vibration intensity criterion is used to conduct the quadratic recognition of the characteristics of vehicle noise and vibration signal, and the method has certain practicability.

2. Correlation Algorithm

2.1. Calculation of Noise and Vibration Signal. The noise and vibration signals are obtained due to the two-dimensional Fourier transform of the third-order cumulant. The calculation process is relatively simple. It can describe the nonlinear characteristics of the vehicle noise and vibration signals in the transmission process. Compared with the power spectrum, the noise and vibration signals can provide the phase. In the information, it has received a lot of references in the characteristic analysis of vehicle noise and vibration signals. In the calculation process of zero mean stable and random, the noise and vibration signals are set as $B_x(\omega_1, \omega_2)$; we can get

$$B_x(\omega_1, \omega_2) = \sum_{\tau_1=-\infty}^{\infty} \sum_{\tau_2=-\infty}^{\infty} c_{3x}(\tau_1, \tau_2) e^{-j(\omega_1\tau_1+\omega_2\tau_2)}. \quad (1)$$

However, in actual engineering, the vehicle noise and vibration signals are all discrete finite signals, and for the discrete determined signal $x(k)$, the following noise and vibration signals can be obtained:

$$\begin{aligned} c_{3x}(\tau_1, \tau_2) &= E\{x(t)x(t+\tau_1)x(t+\tau_2)\}, \\ B_x(\omega_1, \omega_2) &= X(\omega_1)X(\omega_2)X^*(\omega_1+\omega_2). \end{aligned} \quad (2)$$

In the formula, the Fourier transform of the discrete time signal $x(k)$ is performed. According to the nature of dual spectrum, there are six symmetry lines in the range of dual spectrum, symmetry line,$X(\omega_1)\omega_1 = \omega_2 2\omega_1 = -\omega_2$, $2\omega_2 = -\omega_1$, $\omega_1 = -\omega_2$, $\omega_1 = 0$, and $\omega_2 = 0$. As shown in Figure 1, the full-duplex spectral region is divided into 12 regions.

The identification and analysis of vehicle noise and vibration signals are shown in Figure 1, which is divided into two steps [12]:

Step 1. Calculate the energy of each segment of the received signal sequence divided by length $Ny_j = \sum_{i=1}^{N_1} |x_{jN_1} + i|^2 N = N_1 N_2$. Then, it will be used to find the likelihood ratio of the sequential test.

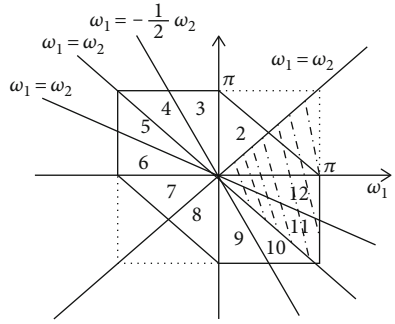

FIGURE 1: Schematic diagram of symmetry axis of noise and vibration signals.

Step 2. Calculate the inspection statistics $\Lambda_K = \sum_{j=1}^{K} \lambda_j y_j$ and $1 \le K \le N_2$, and compare them with the thresholds A and B and make a judgment. If $B < \Lambda_K < A$ is always established and the judgment cannot be made, to ensure that the inspection result is obtained within the limited sampling signal point, we adopt the change. The step size LMS algorithm compares the statistics with the truncation threshold C and makes a decision, namely,

$$\Lambda_{N_2} = \sum_{j=1}^{N_2} \lambda_j \begin{cases} \ge C, & \text{accept } H_1, \\ < C, & \text{accept } H_0. \end{cases} \tag{3}$$

2.2. Analysis of Average Sample Size. Below, we derive and analyze the average sample size of the proposed algorithm in a complex electromagnetic environment and calculate the mathematical expectation for the low signal-to-noise ratio ($\rho \ll 1$) and the likelihood ratio of $N_1 > 10$:

$$\begin{cases} E\left[\lambda_j | H_0\right] \approx -0.5 N_1 \rho^2 - \rho, \\ E\left[\lambda_j | H_1\right] \approx 0.5 N_1 \rho^2 + 0.5\rho. \end{cases} \tag{4}$$

By substituting formula (4) into formula (1), the average capacity samples under the dual hypothesis test conditions can be obtained as follows:

$$\begin{cases} ASN_{H_0} = N_1 E(N_2 | H_0) = -\dfrac{\alpha A + (1-\alpha)B}{0.5\rho^2 + \rho / N_1}, \\ ASN_{H_1} = N_1 E(N_2 | H_1) = \dfrac{(1-\beta)A + \beta B}{0.5\rho^2 + 0.5\rho / N_1}. \end{cases} \tag{5}$$

In summary, the results show the sample ASN, segment length, and received noise ratio of the successive inspection calculation method. Therefore, ASN and N1 want to obtain higher detection results in a complex background, propose the corresponding relationship of the calculation method, and conduct an important discussion on the detection of this performance.

Conclusion 1. When the electromagnetic is in the ($\rho \ll 1$) cognitive network, the calculation method for segmented energy processing uses the average capacity sample ASN, which is affected by the false alarm probability of the system: α and leak detection probability β, and when the received signal-to-noise ratio is proportional to the fragment length, ρ is inversely proportional.

Summarizing to reduce the average sample size of the calculation method, the smaller segment length N1 should be selected first, provided that N1 meets the limiting standard of the central limit.

2.3. Discussion on the Best Truncated Threshold. In the successive inspection algorithm, the inequality $B < \Lambda_K < A$ related to the inspection statistics is always established within a certain inspection time, and the determination may not be possible. In order to obtain the inspection result within the limited inspection time, finally the inspection statistics are compared with the reduced threshold C to obtain the final judgment result. The following analysis of the threshold C will be discussed [13, 14]. The probability density function of the test statistics for checking the statistical quantity, the following inequalities describing the false alarm probability, and the probability of missed detection of the variable step size LMS algorithm are established:

$$\begin{cases} \alpha(N_2) \le \alpha + \dfrac{\exp B - 1}{\exp B - \exp A} \displaystyle\int_C^A f\left(\Lambda_{N_2} | H_0\right) d\Lambda_{N_2}, \\ \beta(N_2) \le \beta + \dfrac{\exp B(1 - \exp A)}{\exp B - \exp A} \displaystyle\int_B^C f\left(\Lambda_{N_2} | H_1\right) d\Lambda_{N_2}. \end{cases} \tag{6}$$

Among them, please refer to the appendix for the detailed derivation process of determining $f(\Lambda_{N_2} | H_0)$ and $f(\Lambda_{N_2} | H_1)$. In order to obtain the best detection performance, $\alpha(N_2) + \beta(N_2)$ must be forced to the minimum value. Therefore, C is selected to minimize the sum of the terms on the right side of the equation, namely,

$$\min G(C) = \frac{\exp B - 1}{\exp B - \exp A} S_0 + \frac{\exp B(1 - \exp A)}{\exp B - \exp A} S_1, \tag{7}$$

where S_0 and S_1, respectively, represent the definite integral term in equation (6). Taking the derivative of equation (7) $G'(C) = 0$ to solve the equation $f(C|H_0)/f(C|H_1) = \exp B(1 - \exp A)/\exp B - 1$, we can approximate the best truncation threshold in the lowest signal-to-noise ratio ($\rho \ll 1$)as

$$C = -0.25 N_2 \rho + (AB + B) \frac{0.25 - \rho N_1 + \rho^2 \left(N_1 + N_1^2\right)}{N_2 (N_1 \rho^2 + 1.5\rho)}. \tag{8}$$

In summary, the received signal is used to divide the energy and analyze the mentioned vehicle noise signal identification and arrange the calculation method. The normal deployment process is detected and merged successively, and the calculation method and reasoning below are relatively simple. At the same time, by adopting the restriction of reduction, it can be determined that the ideal detection result can be obtained from the detection within the specified time range.

3. Recognition and Analysis of Vehicle Noise and Vibration Signals

In the process of vehicle noise and vibration signal recognition, noise interference is mainly caused by transmitter noise. Generally, it refers to abnormal changes caused by the amplitude, frequency, pulse width, and repetition frequency of vehicle noise and vibration signals; that is, the stability of the vehicle noise and vibration signal recognition signal leads to the noise interference. Signal instability can be roughly divided into two types: regularity and randomness. The instability of regularity is mainly caused by insufficient power supply filtering, mechanical jitter, etc. Random instability is the random jitter of the noise generated by the transmitter tube and the modulation pulse.

The noise output from the vehicle noise and vibration signal identification transmitter indicates more non-Gaussian and nonlinear characteristics, and the noise and vibration signal analysis can maintain the amplitude and phase information of the signal, while interference completely suppresses the influence of Gaussian noncolor noise on non-Gaussian signals. Bispectral can be used for the extraction of unconscious modulation features. The concept of the following noise and vibration signals is given.

Assume that the high-order cumulant $c_{kx}(\tau_1, \tau_2, \cdots, \tau_{k-1})$ is absolutely summable, namely,

$$\sum_{\tau_1=-\infty}^{\infty} \cdots \sum_{\tau_{k-1}=-\infty}^{\infty} |c_{kx}(\tau_1, \cdots, \tau_{k-1})| < \infty. \tag{9}$$

The k-order spectrum is defined as the (k-1)-order discrete Fourier transform of the k-order cumulant, namely,

$$S_{kx}(\omega_1, \omega_2, \cdots, \omega_{k-1}) = \sum_{\tau_1=-\infty}^{\infty} \cdots \sum_{\tau_{k-1}=-\infty}^{\infty} c_{kx}(\tau_1, \cdots, \tau_{k-1}) \times \exp\left[-j(\omega_1\tau_1 + \cdots + \omega_{k-1}\tau_{k-1})\right]. \tag{10}$$

Then, the noise vibration signal, the third-order spectrum, can be defined as

$$B_x(\omega_1, \omega_2) = \sum_{\tau_1=-\infty}^{\infty} \sum_{\tau_2=-\infty}^{\infty} c_{3x}(\tau_1, \tau_2) \exp\left[-j(\omega_1\tau_1 + \omega_2\tau_2)\right]. \tag{11}$$

From the noise vibration signal in the estimation, the signal noise oscillation signal including phase noise can be obtained. The discrete noise signal received by the reconnaissance aircraft is $w(n)$ Gaussian white noise signal in the formula of $\mathrm{x(n)} = \mathrm{s(n)} + \mathrm{w(n)}$. $s(n)$ includes the non-Gaussian noise signal output from the transmitter $w(n)$ and $s(n)$, which are independent of each other. Calculate the cumulative amount of $x(n)$ 3 times.

$$c_{3x}(\tau_1, \tau_2) = E\{[s(n) + w(n)][s(n+\tau_1) + w(n+\tau_1)] \cdot [s(n+\tau_2) + w(n+\tau_2)]\}. \tag{12}$$

Expand the formula (4), and then, merge into

$$c_{3x}(\tau_1, \tau_2) = c_{3s}(\tau_1, \tau_2) + c_{3w}(\tau_1, \tau_2) + E[w(n)][c_{2x}(\tau_1) + c_{2x}(\tau_2) + c_{2s}(\tau_2 - \tau_1)] + E[s(n)][c_{2w}(\tau_1) + c_{2w}(\tau_2) + c_{2w}(\tau_2 - \tau_1)]. \tag{13}$$

As long as the mean of the signal and noise is zero, then

$$c_{3x}(\tau_1, \tau_2) = c_{3s}(\tau_1, \tau_2) + c_{3w}(\tau_1, \tau_2). \tag{14}$$

Since $w(n)$ is a Gaussian noise signal, $c_{3w}(\tau_1, \tau_2)$ may not be included in the calculation. Therefore, it can be known that the vehicle noise and vibration signal identification signal can eliminate the white noise through the third-order cumulant, and then, the noise and vibration signals will be determined by $c_{3s}(\tau_1, \tau_2)$, namely,

$$c_{3x}(\tau_1, \tau_2) = c_{3s}(\tau_1, \tau_2) = E\{s(n)s(n+\tau_1)s(n+\tau_2)\}. \tag{15}$$

According to the above analysis, the characteristics of the evaluated vibration signal are mainly composed of the characteristics of the signal itself and non-Gaussian noise. Therefore, the evaluation of the noise and vibration signals in the vehicle noise and vibration signals is mainly based on the unique characteristics of the signal itself, and the unique characteristics of different vehicle noise and vibration signals can also be obtained.

However, if the two-dimensional function can use the full-duplex spectrum as the signal feature and generate a two-dimensional template for matching, the amount of calculation will be very large, which cannot meet the high standard requirements of signal recognition. The key to solving this problem lies in the introduction of high-performance calculation methods for noise and vibration signals. The two-dimensional double spectrum is converted into a one-dimensional function. But, the dual spectrum of high-performance computing also has the following shortcomings.

(1) The realization of high-performance computing dual-spectrum is usually high-performance computing along each path. However, the secondary features calculated by this mode are inconsistent with the results to be recognized, and some dual-spectrum points have a small effect on the results of the recognition target and belong to the ordinary dual spectrum

(2) If there is a cross term in the initial observation signal, the high-order accumulation calculated by using the multicorrelation function will cause the cross term to become more complicated. Because the cross

term is generated randomly, the determined calculation method cannot be used to eliminate cross terms

In order to extract the secondary characteristics of the dual spectrum as the feature of the dual spectrum and eliminate or reduce the disadvantages of the dual-spectrum process of high-performance computing, it can be used as the characteristic parameter of the vehicle noise and vibration signal, and the optimal separability can be obtained in the vibration intensity. This will effectively solve many problems such as cross terms caused by ordinary dual-spectral points and high-performance computing.

Suppose $\{x(n)\}$ if the k-times steady-state random process with an average value of zero and the k-time cumulant of the process are absolutely additable, then the Fourier transform of the k-1 dimensional discrete time defines the k-time spectrum of the signal as k-times cumulant $C_{kx}(\tau_1, \tau_2,\cdots,\tau_{k-1})$ as follows:

$$S_{kx}(\omega_1, \omega_2,\cdots,\omega_{k-1}) = \sum_{\tau_1=-\infty}^{\infty} \cdots \sum_{\tau_{k-1}=-\infty}^{\infty} c_{kx}(\tau_1,\cdots,\tau_{k-1}) \times \exp\left[-j(\omega_1\tau_1+\cdots+\omega_{k-1}\tau_{k-1})\right]. \tag{16}$$

The third-order spectrum $S_{3x}(\omega_1, \omega_2)$ of the signal is called the noise vibration signal, and $B_x(\omega_1, \omega_2)$ is expressed as

$$B_x(\omega_1, \omega_2) = \sum_{\tau_1=-\infty}^{\infty} \sum_{\tau_2=-\infty}^{\infty} c_{3x}(\tau_1, \tau_2) e^{-j(\omega_1\tau_1+\omega_2\tau_2)}. \tag{17}$$

Bispectral estimation is divided into direct method and indirect method [15]. This article mainly uses direct bispectral estimation. The discrete time Fourier transform of $x(n)$ can be expressed in equation (17).

$$B_x(\omega_1, \omega_2) = X(\omega_1)X(\omega_2)X^*(\omega_1 + \omega_2). \tag{18}$$

According to the symmetry of the noise and vibration signal, we can get

$$B_x(\omega_1, \omega_2) = X(\omega_1)X(\omega_2)X(-\omega_1 - \omega_2). \tag{19}$$

The noise and vibration signal graph are 3D, which is not intuitive. The one-dimensional slice of the three-dimensional graph of the noise and vibration signal, that is, the characteristic of the signal to the $\omega = \omega_1 = \omega_2$ vibration signal, is

$$B_x(\omega, \omega) = X(\omega)X(\omega)X^*(2\omega) = X(\omega)X(\omega)X(-2\omega). \tag{20}$$

Use the noise vibration signal method and the vehicle noise method to perform feature extraction on several groups of data, and the required time is shown in Table 1.

As can be seen from Table 1, the dual-spectrum diagonal slicing method greatly reduces the calculation time. The complexity of the algorithm can be greatly reduced only by calculating the diagonal slice, but the dual-spectral slice is a one-dimensional function and cannot represent all the characteristics of the signal. Chirp-Z transformation adjusts the parameters of the spiral line so that the spectrum starts or ends at any point and expands the analysis path to supplement the value of the noise and vibration signals to improve the recognition accuracy. Therefore, the Chirp-Z transformation is used to convert the unit circle of the Z plane into a spiral, and the resulting spiral is used to analyze the signal spectrum.

Table 1: Noise vibration signal method and vehicle noise method feature extraction time.

Algorithm	Number of data sets			
	200	400	800	1000
Noise vibration signal (s)	25.18	37.84	76.19	1o7.9o
Vehicle noise (s)	1o.6o	16.13	27.17	34.49

For discrete time series of finite length $x(n)$, $0 \le n \le N$; the Chirp-Z is

$$X(z) = \sum_{n=0}^{N-1} x(n) z_k^{-n}, 0 \le k \le M - 1. \tag{21}$$

In a few days, z_k is the sampling point of any path on the Z plane:

$$z_k = AW^{-k}, k = 0, 1, \cdots, M - 1. \tag{22}$$

The sampling points deleted in the Z plane, the growth rate of the spiral pass. The angular frequency difference between two similar samples can use any value to obtain the frequency resolution. The number of complex noise vibrations is replaced by MD, while ensuring that the $M >$ of N is not the same; when in the background of N, a detailed analysis of the frequency domain can be achieved. Use Zo's selection to analyze the value of each frequency input. Therefore, when Chirp-Z converts vehicle noise, the complex vehicle noise can be at any point in the Z plane, and the calculation method is more active.

The noise of Chirp-Z conversion can maintain high-level original information, and the calculation can be used immediately. As the calculated data increases, the data processing also increases. In addition, to remove the ordinary noise signal points and crossovers in the noise and vibration, different separation methods are often used to calculate the value of the noise and vibration signal and identify the usability, so as to achieve the reextraction of the vibration signal.

3.1. Vibration Kurtosis Detection. In the literature, as a characteristic parameter in signal classification and recognition, Fisher's separation measurement is used to sort the characteristics of the dual spectrum, and the dual spectrum with

the strongest separation is selected. Fisher measurement is

$$m_{ij}(\omega) = \frac{\sum_{l=i,j} p^{(l)} \left[E_k\left(B_k^{(l)}(\omega)\right) - E_l\left[E_k\left(B_k^{(l)}(\omega)\right)\right]\right]^2}{\sum_{l=i,j} p^{(l)} \operatorname{var}_k\left(B_k^{(l)}(\omega)\right)}, \quad (23)$$

where $p^{(l)}$ is a random variable; $B^{(l)} = B_k^{(l)}(\omega)$ is the prior probability; $E_k(B_k^{(l)}(\omega))$ and $\operatorname{var}_k(B_k^{(l)}(\omega))$ are the mean and variance of the l-th signal at the frequency $\omega = (\omega_1, \omega_2)$, respectively; and $E_l[E_k(B_k^{(l)}(\omega))]$ is the overall center of the sample noise and vibration signals of all signals at the frequency ω.

Fisher can separate the center degree of the entire signal and the ratio of the dispersion to measure the deviation of the average bispectrum on the frequency of a certain signal. If there are two signal centers, the Fisher measurement value is still 0 when the difference with the signal as a whole is small but the dispersion is large. $\omega = (\omega_1, \omega_2)$ cannot show the difference between the two signals. Misjudgments are prone to occur in the classification and recognition process. In other words, the Fisher measurement only reflects the separation between two arbitrary classes or between classes and does not consider the internal distribution characteristics of each class and the separation between one class and the other.

In order to solve this problem, the extended Bali distance can be used as a benchmark for determining the separation of multiple signal types. Vibration intensity is often used for two classification problems [16, 17]. According to the analysis of the above Fisher measurement, the vibration intensity can be expanded as follows.

$$m_{ij}(\omega) = \frac{1}{4} \frac{\left[E_k\left(B_k^{(i)}(\omega)\right) - E_k\left(B_k^{(j)}(\omega)\right)\right]^2}{\sum_{l=i,j} \operatorname{var}_k\left(B_k^{(l)}(\omega)\right)} + \frac{1}{2} \ln \left\{ \frac{\sum_{l=i,j} \operatorname{var}_k\left(B_k^{(l)}(\omega)\right)}{2\prod_{l-i,j} \operatorname{var}_k\left(B_k^{(l)}(\omega)\right)^{1/2}} \right\}. \quad (24)$$

The greater the Bali distance between the two signals (i, j), the better the separability of the sample. The extended variable distance measurement (hereinafter referred to as BM) is used to filter the bispectral values of valuable measurement objects. After resorting, the strongest type of separable value can be selected as the feature vector for signal classification and recognition.

Suppose there are a total of C-type signals to be identified, and the k-th group of observation data of the l-th signal is $X_k^{(l)}(1), X_k^{(l)}(2), \cdots, X_k^{(l)}(N)$, where N is the number of sampling points, $l = 1, 2, \cdots, C$ and $k = 1, 2, \cdots, N_l$ (N_l is the number of observation data of the l-th signal). The feature vector extraction steps based on complex vehicle noise are the following:

(a) Calculate the vehicle noise value $B(\omega, \omega)$ of the signal

(b) Set the various parameters in the Chirp-Z transformation. $A_0 = 1$, $W_0 = e^{-j2\pi/N}$, and M = N are used in the paper; that is, the signal vehicle noise is calculated on the unit circle of the Z plane

(c) Use equation (10) to calculate the extended vibration intensity $m_{ij}(\omega)$ of all possible category combinations (i, j). According to the calculated extended vibration intensity value, the noise vibration signal can be divided into available noise vibration signal and unrelated noise vibration signal; it is defined as

$$B(\omega) \in \begin{cases} B_l, m_{ij}(\omega) > \lambda_{ij}, \\ B_N, m_{ij}(\omega) \le \lambda_{ij}, \end{cases} \quad (25)$$

where in order to determine the useful and irrelevant extended vibration intensity threshold of the noise vibration signal λ_{ij}, the threshold is obtained through a large number of simulation experiments

(d) The classified information of the noise vibration signal B_l including (i, j) type signals in the selected $m_{ij}(\omega)$ is sorted by using the M largest extended vibration intensity values

$$m_{ij}(\omega_1) \ge m_{ij}(\omega_2) \ge \cdots \ge m_{ij}(\omega_M) \quad (26)$$

(e) Normalize the extended vibration intensity measurement value $m_{ij}(\omega)$:

$$\bar{m}_{ij}(\omega_p) = \sqrt{\frac{m_{ij}(\omega_p)}{\sum_{k=1}^{M} \left[m_{ij}(\omega_k)\right]^2}}, \quad p = 1, 2, \cdots, M, \quad (27)$$

where $\bar{m}_{ij}(\omega_p)$ is the useful quantity n_{ij} of the representative vector between the signal (i, j) categories. The corresponding frequency $\{\omega_{ij}(p), p = 1, 2, \cdots, n_{ij}\}$ is a useful frequency. For other (i, j) types, the same effective frequency is acquired once

(f) Using favorable frequencies, combine the useful frequencies that can be separated from the n_{ij} strongest classes of the finally selected i-th signal into a series of $\{\omega_{ij}(q), q = 1, 2, \cdots, Q\}$, and combine all the corresponding selected complex vehicle noise values with the sequence $\{Z_k^{(l)}(q), q = 1, 2, \cdots, Q\}$. When $Q = \sum_{(i,j)} n_{ij}, k = 1, 2, \cdots, N_l$, the vector of the l-th signal is displayed as $\{Z_k^{(l)}(q), q = 1, 2, \cdots, Q\}$

(g) Pass the acquired feature vector to the classifier to be able to classify and recognize

3.2. Use Wavelet to Achieve Signal Denoising. If $\varphi(t) \in L^2(R)$, $\varphi(w)$ is its Fourier transform, when the allowable conditions are

$$Cw = \int_R \frac{|\varphi(w)|^2}{|w|} dw < \infty. \tag{28}$$

φ is called as a wavelet generating function.

The wavelet transform of any function $f(t) \in L^2(R)$ is defined as

$$WT_f(a,b) = \frac{1}{\sqrt{a}} \int_{-\infty}^{\infty} f(t)\varphi^*\left(\frac{t-b}{a}\right) dt, \quad a > 0. \tag{29}$$

In the formula, a is the scale factor and b is the time shift factor. The function of the scale factor is to stretch the wavelet function for multiresolution analysis.

In the multiresolution analysis and signal time-domain decomposition, binary discrete wavelet transform is widely used; that is, $a = 2^j$, $j \in z$ is taken, so the binary wavelet transform is obtained as

$$WT_{2j}(b) = 2^{-j/2} \int_R f(t)\varphi\left(\frac{b-t}{2^j}\right) dt. \tag{30}$$

The original signal can be reconstructed by dyadic wavelet transform, namely,

$$f(t) = \sum_{j\in z} \int_R WT_{2j}(b)\varphi_{2j,b}(t) db. \tag{31}$$

Why does the inverse wavelet function φ C(R) have n vanishing moments, then $\forall x \in (x_0 - \delta, x_0 + \delta)$, there is

$$\left|\left(W_\varphi f\right)(a,b)\right| \le K * a^\alpha. \tag{32}$$

Formula (5) points out that as the scale increases, the amplitude value after wavelet transform shows a power increasing trend relative to the singularity greater than zero, and for the singularity less than zero, the amplitude value shows a decreasing trend. The smoothing of the signal is usually preferred, the singularity index at the singularity point is usually greater than zero, and the noise has a negative singularity index. In this way, when the scale of the wavelet transform increases, the mixed noise and the signal show completely different change characteristics, and the signal and noise can be separated based on these characteristics.

(1) Wavelet decomposition of one-dimensional signal

(2) Noise reduction processing

Select wavelet, determine the number of wavelet decomposition levels N, and perform N-level wavelet decomposition on the signal.

There are roughly three processing methods for noise removal processing of the decomposed high-frequency coefficients.

(a) Forced noise cancellation: change the high-frequency coefficients to 0

(b) Default threshold denoising: select the default threshold for processing

(c) Provide soft/hard threshold noise elimination: the threshold is obtained by empirical formula, and its value is more reliable than the default threshold

(3) The wavelet reconstruction of one-dimensional signal is based on the equation

(4) The signal is reconstructed according to the wavelet coefficients of each layer after processing

3.3. Vehicle Vibration Signal Detection Algorithm. Vehicle vibration signal detection uses vibration signals to determine whether there is a target. Based on the characteristics of the target and noise vibration signal, two actual detection algorithms based on negative entropy and detection algorithm based on power spectrum distribution are proposed.

When the vehicle is running, the excitation added to the wheels and tracks is a multifrequency stable excitation, and the distance between the seismic source and the sensor changes with time, so the sensor measures the superposition of harmonics of each frequency.

The seismic waves caused by vehicle movement are continuous seismic waves, which mainly depend on the self-vibration of the frame suspension system, the vibration of the engine and the transmission system, and the excitation of the undulating ground caused by the driving of the vehicle. The signal is dominated by low-frequency components, and the main peak frequency is about 100 Hz. Figure 2 shows the time-domain waveform of the vehicle vibration signal.

Entropy is an important metric to measure non-Gaussianity from an informatics point of view, and it can effectively distinguish Gaussian signals from non-Gaussian signals. The entropy of the discrete random variable X can be defined as

$$H(x) = -\sum_i P(X = a_i) \lg P(X = a_i). \tag{33}$$

In the formula, a_i is the value of X.

There are two problems with the application of entropy:

(1) An algorithm is picky about the type of noise, and the limiting noise must be Gaussian or Gauss-like noise

(2) The algorithm still needs accurate posterior information to determine the threshold

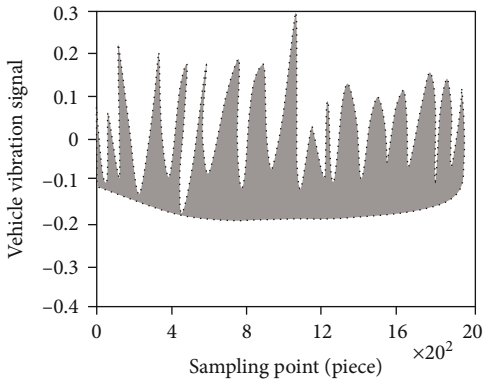

Figure 2: Time-domain waveform of vehicle vibration signal.

The difference between negative entropy and entropy is that the value of negative entropy relative to Gaussian variables is zero, while the value of non-Gaussian variables is always nonnegative, and negative entropy does not change with the change of signal amplitude. According to the above characteristics, the algorithm based on the negative entropy characteristic can set the threshold value in advance through a large amount of statistical information and can obtain a good detection effect without the need for a posteriori information adjustment. The definition of negative entropy J is as follows.

$$J(x) = H\left(X_{\text{gauss}}\right) - H(x) \tag{34}$$

In the formula, X_{gauss} is a Gaussian random vector, which has the same mean and covariance matrix as x; the value of x_{gauss} can be estimated by the following formula:

$$H\left(X_{\text{gauss}}\right) = \frac{1}{2}\lg\left|\det\sum\right| + \frac{n}{2}[1 + \log 2\pi]. \tag{35}$$

In the formula, n is the dimension of the vector; Σ is the covariance matrix.

Since the calculation of negative entropy depends on factors such as the preprobability density of random variables, the analysis of negative entropy is only maintained at the theoretical stage. In practical applications, an approximate formula based on the following high-order cumulants is usually used to calculate negative entropy.

$$J(x(t)) \approx \frac{1}{12}E\left\{x^3(t)\right\}^2 + \frac{1}{48}K^2. \tag{36}$$

In the formula, E is the mathematical expectation of a random variable. K is the peak of the random variable x:

$$K = \frac{E\left\{x^4(t)\right\}}{E^2\left\{x^2(t)\right\}} - 3. \tag{37}$$

For steady-state random signals, signal power spectrum analysis is one of the commonly used methods in frequency domain analysis. The seismic signals caused by vehicles within a certain distance range can be approximated as generalized and stable. In modern signal analysis, sample data can be used to estimate the power spectral density of a steady-state random signal, which is one of the important research contents of digital signal processing. The welch method is used to estimate the power spectrum.

The power spectrum is defined as the Fourier transform of the autocorrelation function, and the autocorrelation function is an important statistic of a random signal and is defined as follows.

$$r_X(m) = E\{X^*(n)X(n+m)\}. \tag{38}$$

The definition of the power spectrum is the Fourier transform of the autocorrelation function, namely,

$$P_X\left(e^{jw}\right) = \sum_{-\infty}^{\infty} r_X(m)e^{-jwm}. \tag{39}$$

Welch power spectrum estimation algorithm

(1) Divide N data into L segments; each segment of M data is $N = M * L$

(2) Choose an appropriate window function $w(n)$, use this function to weight each segment of data accordingly, and determine the periodogram of each segment by formula (13)

$$I_M^i(w) = \frac{1}{MU}\left|\sum_{0}^{M-1} x_i(n)w(n)e^{-jwn}\right|^2. \tag{40}$$

In the formula, $U = 1/M\sum_{n=0}^{M-1}w^2(n)$ is the normalization factor.

(3) Averaging the segmented periodogram to obtain the signal power spectrum, namely,

$$P_{xx}(w) = \frac{1}{L}\sum_{i=1}^{L} I_M^i(w) \tag{41}$$

Figures 3 and 4 are the power spectra of the vehicle vibration signal and the environmental noise vibration signal.

It can be seen from the above power spectrum distribution that the vibration signal of the vehicle is mainly concentrated below 300 Hz, the power spectrum of the noise vibration signal is relatively stable, and the energy is small, so the threshold value within 0~500 Hz is selected, and the power spectrum on both sides of the threshold value is calculated. The energy-to-energy ratio can be used as a benchmark to distinguish between noise and target.

Vehicle vibration signal detection algorithm based on welch power spectrum

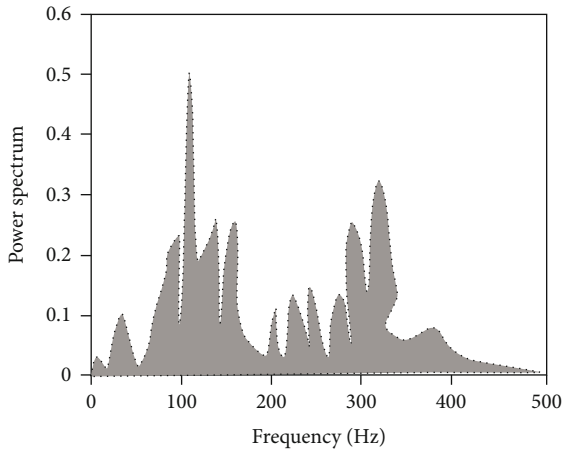

Figure 3: Power spectrum of vehicle vibration signal.

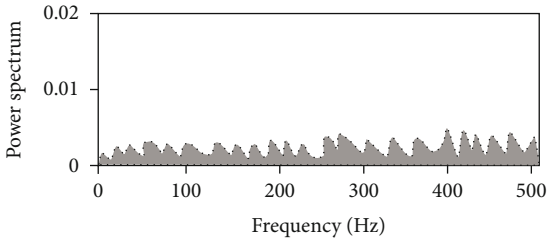

Figure 4: Power spectrum of noise vibration signal.

(1) Estimate the signal power spectrum

(2) Choose the threshold N and the energy ratio to determine the threshold, and calculate the average energy of the power spectrum on both sides of the threshold:

$$P_L = \frac{1}{N}\sum_{n=0}^{N} P^2(f),$$
$$P_H = \frac{1}{500-N}\sum_{n=N}^{500} P^2(f), \quad (42)$$
$$r = \frac{P_L}{P_H}$$

(3) If $r < r_0$, no target appears, and if $r > r_0$, then a target appears

4. Simulation Results

The power amplifier is a key component in the radio frequency transmitter, and the slight difference in its hardware is one of the main sources of the subtle characteristics of the signal, and it can generate vehicle noise and vibration signals through the modeling, analysis, and simulation of functional behavior. The modeling of functional behavior does not need to consider the functional circuit structure and component characteristics, and it is more convenient only by analyzing the relationship between signal input and system response. General functional modeling models include nonstorage models suitable for narrowband signals, including storage models suitable for wideband signals, for example, the memory polynomial model and Voltera model. Please select memory polynomial (MP). The model generates a simulated vehicle noise and vibration signal. When the system input signal is $x(n)$ and the output signal is $y(n)$, the system responds to it as follows:

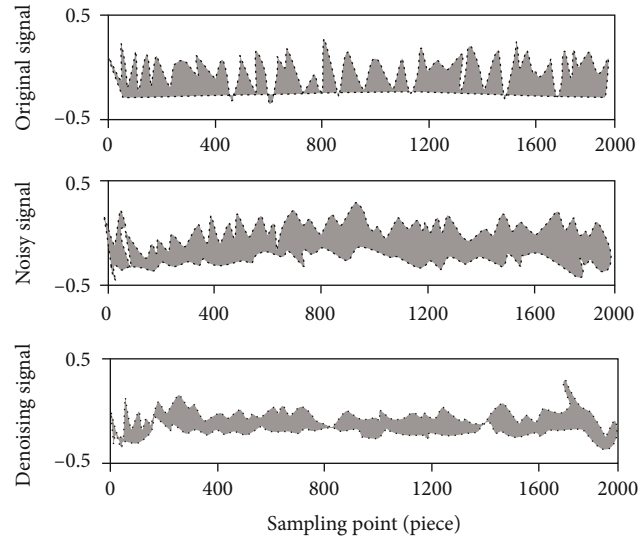

Figure 5: Wavelet denoising of vehicle vibration signal.

$$y(n) = \sum_{i=1}^{I}\sum_{j=1}^{J} a_{ij}x(n-j)|x(n-j)|^{i-1}. \quad (43)$$

For the same input signal $x(n)$ in the modulation mode, assuming different types of model parameters a_{ij}, different noise and vibration signals with nonlinear characteristics can be obtained. The input signal $x(n)$ represents the frequency band modulation of the signal, which can be expressed as

$$x(n) = s(n)e^{j2\pi(f_c/f_s)}, \quad (44)$$

where $s(n)$ represents the baseband modulation signal, f_s represents the process sampling frequency of the vehicle noise and vibration signals, and f_c represents the carrier frequency of the vehicle noise and vibration signal. The baseband signal $S(n)$ is the QPSK modulation used in this article, the signal sampling frequency f_s is set to 20 MHz, the signal carrier frequency f_c is set to 4 MHz, and the value of the symbol rate is set to R_B=2 MHz. In this article, the polynomial order I corresponding to the signal power amplifier is set to 3, and the delay order J is set to 3. Then, for the signal power amplifier, model coefficients can be

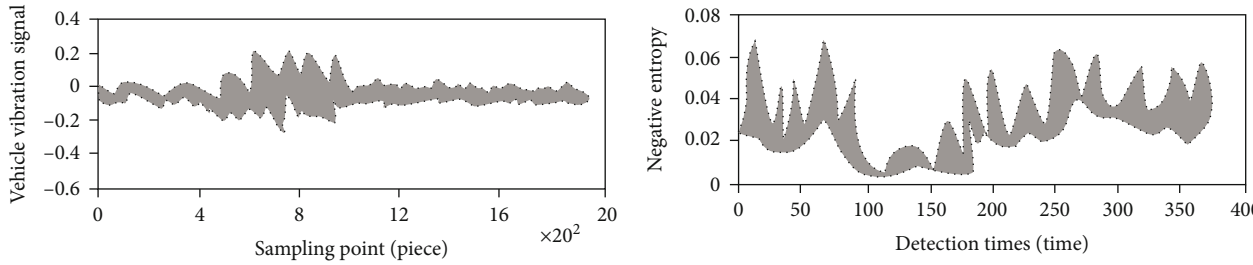

(a) Vibration signal of the vehicle to be detected

(b) Negative entropy test results

Figure 6: Negative entropy of vehicle vibration signal.

Table 2: Vehicle vibration signal detection results under different signal-to-noise ratio conditions.

Signal-to-noise ratio (dB)	Detection method	Correct detection rate (before denoising)	Correct detection rate (after denoising)
4	Negative entropy detection	100%	100%
	Power spectrum distribution detection	100%	100%
-2	Negative entropy detection	75%	90%
	Power spectrum distribution detection	100%	100%
-5	Negative entropy detection	50%	80%
	Power spectrum distribution detection	90%	100%

expressed as

$$A^m = \begin{bmatrix} a_{11}^m & a_{12}^m & a_{13}^m \\ a_{21}^m & a_{22}^m & a_{23}^m \\ a_{31}^m & a_{32}^m & a_{33}^m \end{bmatrix} = \begin{bmatrix} a_{i_1}^m \\ a_{i_1}^m \\ a_{i_1}^m \end{bmatrix} \left[a_{j_1}^m \, a_{j_2}^m \, a_{j_3}^m \right]. \tag{45}$$

The processed data is the vehicle vibration data collected on the spot and part of the data in the SENSIT database. The process is described as going from no target to there, or even disappearing of the target. The sampling frequency is Fs =1000 Hz, and 1928 points are one frame of data.

The wavelet adopts db3 wavelet to carry out 3-layer decomposition, and the soft thresholds are, respectively, 1.456, 1.832, and 2.786. Figure 5 shows the effect diagram of wavelet noise removal of vehicle vibration signal.

The negative entropy detection threshold detects 0.02 and 50 points once, the power spectrum detection threshold N is 300, and the energy ratio discrimination threshold is 10,000. r_0 Figure 6(a) and Figure 6(b) show the negative entropy detection results for detecting the vibration signal of the vehicle.

Collect 20 typical samples for simulation; false alarms and missed alarms in the detection process are all false detections. Table 2 compares the detection results of the two detection algorithms under different signal-to-noise ratio conditions.

It can be seen from the simulation results that wavelet noise elimination can improve the accurate detection rate. As the noise increases, the performance of the negative entropy detection algorithm is reduced, and the performance of the power spectrum distribution detection algorithm is stable, and accurate detection rate is high.

5. Conclusion

On the premise of the conclusion of noise source identification, the noise reduction improvement test is carried out for the vehicle. The sound insulation between the engine compartment and the passenger compartment is strengthened to reduce the transmission of engine noise from the engine compartment to the passenger compartment. Based on the in-depth analysis of the vibration signal characteristics of the diagonal slice of vehicle noise vibration signal degree, the obtained vibration intensity is optimized by using the extended vibration intensity criterion, and the implementation method is introduced. The correlation between different signals is studied, and the recognition method of different signals is given. It is simpler and more effective than the traditional analysis method for vehicle noise and vibration source identification and provides a new test means for the research of vehicle vibration and noise control. By using the actual analysis, the test results show that the use time of the proposed method is reduced and can also be used in multiple types of vehicle noise and vibration signals. The obtained vibration signal characteristics can always have good robustness in the case of low signal-to-noise. When the signal-to-noise ratio is 0, the recognition rate of vehicle noise vibration signal can be greater than 90%.

Data Availability

The data used to support the findings of this study are available from the corresponding author upon request.

Conflicts of Interest

The author declares no conflicts of interest.

Acknowledgments

This research study is sponsored by the National Natural Science Foundation of China. The name of the project is Research on Quantitative Reconstruction of Vehicle Sound Source Based on Aperture Error Correction Kirchhoff Diffraction Acoustic Holography. The project number is 51805229. Thanks are due to the project for supporting this article!

References

[1] P. C. Guillevic, A. Olioso, S. J. Hook, J. B. Fisher, J.-P. Lagouarde, and E. F. Vermote, "Impact of the revisit of thermal infrared remote sensing observations on evapotranspiration uncertainty—a sensitivity study using ameriflux data," *Remote Sensing*, vol. 11, no. 5, p. 573, 2019.

[2] C. Wu, L. Zhang, and L. Zhang, "A scene change detection framework for multi-temporal very high resolution remote sensing images," *Signal Processing*, vol. 124, pp. 184–197, 2016.

[3] G. Notesco, Y. Ogen, and E. Ben-Dor, "Mineral classification of makhtesh ramon in Israel using hyperspectral longwave infrared (lwir) remote-sensing data," *Journal of Remote Sensing*, vol. 7, no. 9, pp. 12282–12296, 2015.

[4] A. Ansari, H. Danyali, and M. S. Helfroush, "Hs remote sensing image restoration using fusion with ms images by em algorithm," *IET Signal Processing*, vol. 11, no. 1, pp. 95–103, 2017.

[5] X. Zhang, "Research on remote sensing image de□aze based on GAN," *Journal of Signal Processing Systems*, vol. 73, pp. 620–627, 2021.

[6] W. G. So and H. K. Kim, "The influence of drama viewing on online purchasing intention: an empirical study," *Journal of System and Management Sciences*, vol. 10, no. 2, pp. 69–81, 2020.

[7] F. Bode, W. Nowak, and M. Loschko, "Optimization for early-warning monitoring networks in well catchments should be multi-objective, risk-prioritized and robust against uncertainty," *Transport in Porous Media*, vol. 114, no. 2, pp. 261–281, 2016.

[8] Liu, & P., "Development and application of fire safety monitoring and early warning system for small and medium sized hospital enterprises," *Basic & clinical pharmacology & toxicology.*, vol. 119, Suppl.4, pp. 57–57, 2016.

[9] C. Hua, Y. Tang, M. Ren, and W. Lin, "Single near-infrared fluorescent probe with high- and low-sensitivity sites for sensing different concentration ranges of biological thiols with distinct modes of fluorescence signals," *Chemical Science*, vol. 74, no. 1, pp. 914–923, 2016.

[10] Y. Z. Liu, Y. S. Zou, Y. L. Jiang, H. Yu, and G. F. Ding, "A novel method for diagnosis of bearing fault using hierarchical multi-tasks convolutional neural networks," *Shock and Vibration*, vol. 2020, no. 13, pp. 1–14, 2020.

[11] C. T. Chiang and K. Y. Liu, "A cmos wearable infrared light intensity digital converter for monitoring unplanned self-extubation of patients," *IEEE Sensors Journal*, vol. 14, no. 16, pp. 136–154, 2019.

[12] W. de Sousa Junior, J. Montevechi, R. Miranda, F. Rocha, and F. Vilela, "Economic lot-size using machine learning, parallelism, metaheuristic and simulation," *Int. Journal of Simulation Modelling*, vol. 18, no. 2, pp. 205–216, 2019.

[13] T. D. Almeida, J. Nacif, F. P. Bhering, and J. R. Junior, "Doctrams: a decentralized and offline community-based traffic monitoring system," *IEEE Transactions on Intelligent Transportation Systems*, vol. 20, no. 3, pp. 1160–1169, 2019.

[14] B. Cian, M. Suzanne, K. Heard, Q. Peter, S. G. Yeates, and V. Aravind, "Nanoscale infrared identification and mapping of chemical functional groups on graphene," *Carbon*, vol. 139, pp. 317–324, 2018.

[15] Singh, & Goyal., "An improved coupled framework for glacier classification: an integration of optical and thermal infrared remote-sensing bands," *International Journal of Remote Sensing*, vol. 39, no. 20, pp. 6864–6892, 2018.

[16] A. J. Barclay, A. Mckellar, and N. Moazzen-Ahmadi, "Infrared observation of a new mixed trimer, co – (co 2) 2Infrared observation of a new mixed trimer, CO – (CO2)2," *Chemical Physics Letters*, vol. 677, pp. 127–130, 2017.

[17] L. Hua and G. Shao, "The progress of operational forest fire monitoring with infrared remote sensing," *Journal of Forestry Research.*, vol. 28, no. 2, pp. 215–229, 2017.